Supercritical Fluid Flow Injection

By G. Ribert⋆, M. Jarczyk§, C. A. Niedermeier¶, X. Petit⋆†, M. Pfitzner§, M. Schmid∗ AND T. Sattelmayer∗

⋆ CORIA - UMR6614 CNRS, INSA de Rouen, Campus du Madrillet
76801 St-Etienne-du-Rouvray, France
§ Institut für Thermodynamik, Universität der Bundeswehr München
Werner-Heisenberg-Weg 39, 85577 Neubiberg, Germany
¶ Lehrstuhl für Aerodynamik und Strömungsmechanik, TU München
Boltzmannstr. 15, 85748 Garching b. München, Germany
∗ Lehrstuhl für Thermodynamik, TU München
Boltzmannstr. 15, 85748 Garching b. München, Germany

Supercritical fluid flow injection is numerically studied based on Mayer's experiment, i.e., a cold nitrogen injection inside a warm, steady nitrogen environment. Three numerical codes featuring different methodologies (compressible or incompressible LES, ILES) are used with equivalent thermodynamics models. Comparisons with experimental data lead to promising results but they still need to be improved as a long time of convergence is required because of the low-speed injection.

1. Introduction

The domain of interest of the present project is the aerospace science and technology where supercritical fluids are considered as propellants. High-pressure combustion in liquid rocket or jet engines poses various technological and scientific difficulties, including injection optimization, atomization, mixing, ignition, flame stabilization, and combustion instabilities. The whole process is so complex that its mechanism cannot be thoroughly understood without extensive theoretical, numerical and experimental works conducted on simplified configurations and under well-controlled conditions. Mixture formation is one of the most important phenomena in liquid rocket combustion devices because it determines combustion efficiency, stability, and heat transfer characteristics. This process is realized through the use of propellant injectors, such as coaxial injector geometries, that have to efficiently operate for different conditions: startup, thrust variation, shutdown. Among the different attempts to provide useful data (mainly density) on supercritical fluid injection, few experiments are available [1–4]. In the present project, Mayer's experiment [4] will be simulated with three different numerical codes that share similar thermodynamics. This specific point is crucial when dealing with supercritical fluids and it will be detailed in section 2.

In Mayer's experiment (see Fig. 1) cold nitrogen is injected into a warm nitrogen environment under different ambient and injection conditions. The diameter of the injector is 2.2 mm. The inlet temperature of the injected fluid can be as low as 90 K; inlet velocities can vary from 1 to 20 m/s according to the considered case. Pressure may vary

† also with CNES.

Investigated Cases	Case 3	Case 4
Injection velocity, m/s	4.9	5.4
Injection temperature, K	126.9	137
Chamber pressure, bar	39.7	39.7
Chamber temperature, K	298	298

TABLE 1. Initial conditions.

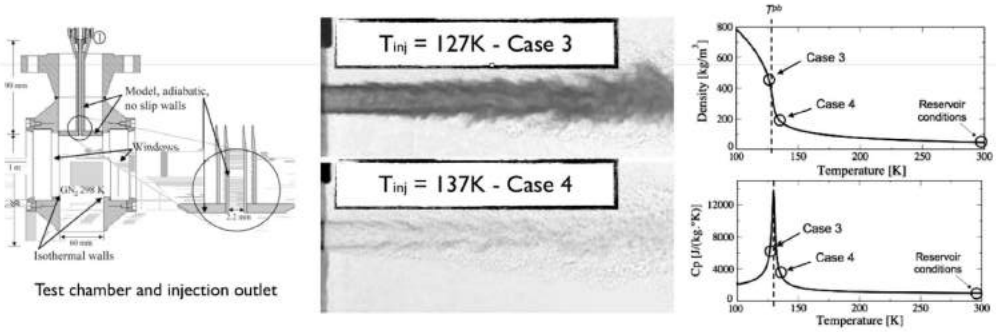

FIGURE 1. Mayer's configuration with experimental visualization (from [4]).

from 3.95 to 6 MPa. Case 3 and 4 as reported in [4] and detailed in Tab. 1 are here under study. Objective of this project is to give insights to the behavior of supercritical jets. This attempt will be realized through different numerical tools: compressible LES (project 1), implicit LES (project 2), low-Mach number assumption (project 3). Finally, acoustic excitation of such jets will be studied in project 4.

2. Thermodynamics

To simulate supercritical fluids, the compressible Navier-Stokes equations for perfect gases have to be modified as follows: a real-gas equation of state (EoS) that accounts for phase change must be implemented, while thermodynamics coefficients as well as transport models are pressure-dependent [5]. All the numerical codes used in this project follow Meng and Yang's [6] or Bellan's [7] recommendations for real-gas thermodynamics. A cubic EoS such as the Soave-Redlich-Kwong (SRK) or Peng-Robinson (PR) EoS (Eq. (2.1)) replaces the classical perfect gas law; a general form may be written as follows [5]:

$$p = \frac{\rho R T}{W - \rho b} - \frac{\rho^2 a\alpha(T)}{W^2 + ubW\rho + wb^2\rho^2} \ , \tag{2.1}$$

where EoS characteristics are given in Tab. 2 for any species k. p stands for pressure, ρ for density and T for temperature. R is the universal gas constant and W the molecular weight of the fluid mixture. The two parameters, $a\alpha$ and b, taking into account the effects

Equation	u	w	b_i	a_i	$\alpha_i(T)$
SRK	1	0	$\frac{0.08664 R T_{c_k}}{P_{c_k}}$	$\frac{0.42748 R^2 T_{c_k}^2}{P_{c_k}}$	$[1+S_i^{\mathrm{SRK}}(1-\sqrt{T/T_{c_k}})]^2$
PR	2	-1	$\frac{0.07780 R T_{c_k}}{P_{c_k}}$	$\frac{0.457235 R^2 T_{c_k}^2}{P_{c_k}}$	$[1+S_i^{\mathrm{PR}}(1-\sqrt{T/T_{c_k}})]^2$

TABLE 2. Coefficients of cubic equations of state.

of attractive and repulsive forces among molecules, respectively, are calculated with the following mixing rules,

$$a\alpha = \sum_{i=1}^{N_s}\sum_{j=1}^{N_s} X_i X_j \alpha_{ij} a_{ij}, \quad \alpha_{ij} a_{ij} = \sum_{i=1}^{N_s}\sum_{j=1}^{N_s} \sqrt{\alpha_i \alpha_j a_i a_j}(1-\kappa_{ij}), \quad b = \sum_{i=1}^{N_s} X_i b_i, \quad (2.2)$$

where X_k is the mole fraction of species k (among N_s species) and κ_{ij} the binary interaction coefficient. The constants a_i and b_i are given in Tab. 2 according to the desired EoS; T_{c_k} and p_{c_k} represent the critical temperature and pressure of species k, respectively. The third parameter, α_i, is a function of the acentric factor, ω_i:

$$S_i^{\mathrm{SRK}} = 0.48508 + 1.5517\omega_i - 0.15613\omega_i^2 \ , \quad (2.3)$$

$$S_i^{\mathrm{PR}} = 0.37464 + 1.54226\omega_i - 0.26992\omega_i^2 \ . \quad (2.4)$$

Both EoS give equivalent results as shown in [8]. Finally, classical techniques used to evaluate transport properties (viscosity and thermal conductivity) are replaced by accurate high-pressure relations proposed by Chung *et al.* [9], which extends the Chapman-Enskog theory by introducing a dense-fluid correction. The binary mass diffusivity are predicted by the Takahashi method [10]. Real-gas simulations (RGS) are now detailed.

3. RGS with SiTCom-B (Project 1)

SiTCom-B (Simulation of Turbulent Combustion with Billions of points [11]) is a finite volume code that solves the unsteady compressible reacting Navier-Stokes equations system on cartesian meshes. It is mainly designed to perform DNS and highly resolved LES on thousands of processors. For the present case, SiTCom-B numerical code has been used with: 4th order central difference schemes and Runge-Kutta time-discretization (4th order); full multi-species formulation with realistic thermodynamics and transport properties; SRK EoS; NSCBC boundary treatment.

The three-dimensional mesh design used for Mayer's experiment is given in Fig. 2. Only a small part of the combustion chamber is simulated to save the time of calculation, but boundary conditions are adapted to still have a representative simulation of the configuration. Injection is prescribed by a turbulent pipe profile discretized on 34 mesh points. The Smagorinsky subgrid scale model is used with the constant fixed to 0.15. In Figs. 3, velocity and schlieren instantaneous flow fields are provided: In Fig. 3(a) the maximum velocity is found in the injection plane because of the inlet turbulent profile. Then, the jet destabilizes and naturally opens leading to pockets of dense fluid and small

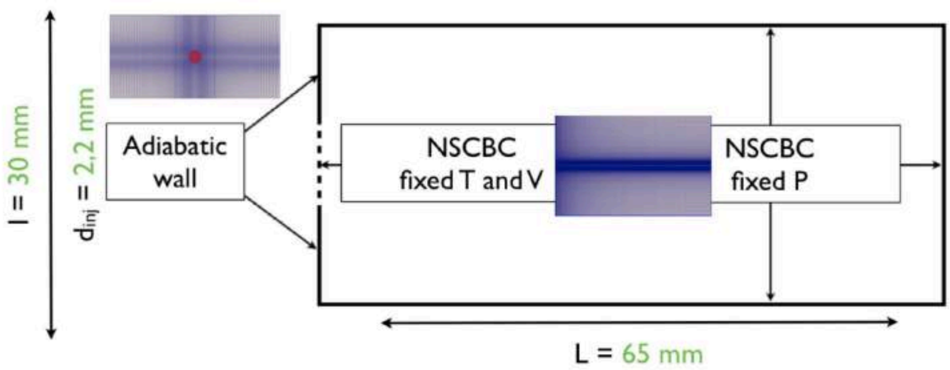

FIGURE 2. Mesh design used in SiTCom-B: $L_x \times L_y \times L_z = 65\,mm \times 15\,mm \times 15\,mm$ with $N_x \times N_y \times N_z = 344 \times 184 \times 184 \approx 11.6$ millions of points.

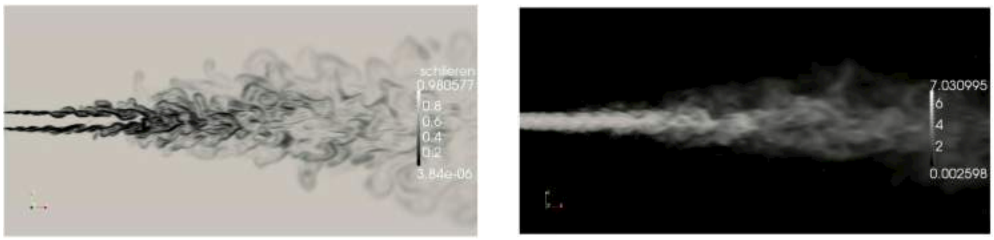

(a) Schlieren. (b) Velocity magnitude (in m/s).

FIGURE 3. Simulation of case 4 with SiTCom-B numerical code.

structures that seems to extract from the main jet (Fig. 3(a)) similarly to those recently observed in two-dimensional simulations [12, 13].

4. RGS with INCA (Project 2)

In this work, we follow two distinct modeling approaches: While within projects 1 and 3 explicit LES is used, project 2 uses Implicit LES (ILES) with the Adaptive Local Deconvolution Method (ALDM). The basic idea of ILES is to directly use the truncation error of the unmodified equations for conservation of mass, momentum and energy. ALDM incorporates free parameters in the discretization scheme which can be used to control the truncation error. A physically motivated implicit SGS model that is consistent with turbulence theory is obtained through parameter calibration, see Ref. [14].

INCA is a general-purpose multi-physics solver for Direct Numerical Simulation (DNS) and Large Eddy Simulation (LES), used by the *I*nstitute of Aerodynamics and Fluid Mechanics at *T*echnische Universität München [15]. ALDM is implemented in INCA for Cartesian collocated grids and used to discretize the convective terms of the Navier-Stokes equations (see Ref. [16] for a detailed description). The diffusive terms are dis-

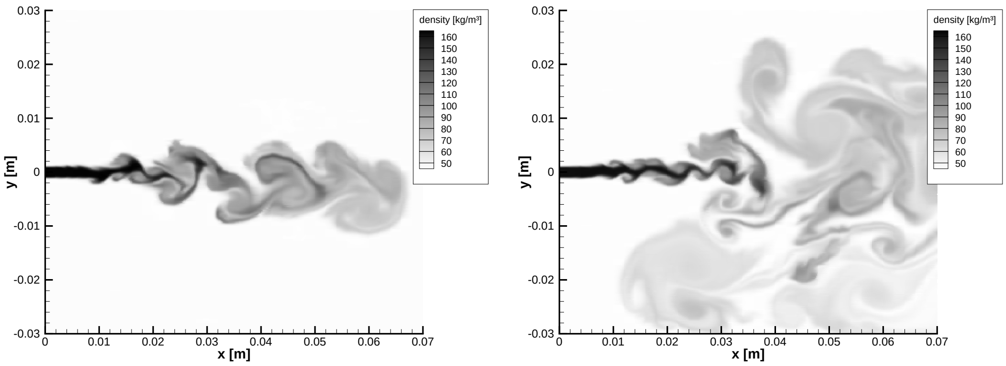

(a) Simulation time 1.8 ms. (b) Simulation time 4.9 ms.

FIGURE 4. Density distribution in the domain.

cretized by 2nd order centered differences and a 3rd order explicit Runge-Kutta method is used for time integration.

A transitional mixing layer of hydrogen and oxygen studied by Okong'o *et al.* [17] was used as a test case in our previous works [18, 19] for successfully validating INCA in terms of real-gas thermodynamics and general applicability for the simulation of supercritical flows. During the summer program, the computational framework was extended in several ways to meet additional needs for simulating Mayer's experiment:

– several boundary conditions (BC) were extended to the simulation of supercritical flows, like an isothermal wall BC, a subsonic jet inflow BC and a constant pressure outflow BC

– the method of Chung *et al.* [9] was implemented for determination of the transport properties

– the robustness of the iterative computation of temperature and pressure was increased for use in near- and transcritical regimes.

A two-dimensional simulation of case 4 was conducted as a proof of concept for the implemented extensions. The domain with a size of $L_x \times L_y$ = 0.55 m $\times$ 0.06 m was discretized with $N_x \times N_y$ = 400 $\times$ 300 = 120,000 cells. While the cell size up to a streamwise coordinate of x = 0.07 m is quadratic and uniform, the streamwise cell size between x = 0.07 m and x = 0.55 m increases linearly with a stretching factor of 1.12 with the spanwise cell size remaining constant. According to the experiment, the upper and lower boundaries are treated as isothermal walls with a fixed temperature of T = 298 K. The upstream boundary is a combination of an adiabatic wall with a jet inflow condition. The temperature of the jet is T_{inj} = 137 K and the velocity is prescribed according to a pipe flow profile with superimposed random fluctuations as in project 1. To save computational time and because the goal of the simulation was a proof of concept and not the eventual comparison with experimental data, the average inflow velocity was set to 54 m/s instead of 5.4 m/s. Finally, the downstream boundary condition is an outflow with a fixed pressure of p = 3.98 MPa.

Figures 4 show the density distribution in the domain after 1.8 ms and 4.9 ms, respectively. First, the jet develops very nicely and the typical structures stemming from Kelvin-Helholtz rollups can be observed. However, severe backflow above and below the jet core is present at the later timestep, preventing the jet from developing like in the experiment. This behaviour can be explained with the two-dimensionality of the simulation, which replicates in fact a flat jet instead of a round jet. For a flat jet, the spreading angle is not constant but increases downstream and much more entrainment can be observed. This is in agreement with the results from the simulation, because the backflow at the top and the bottom of the domain is directly caused by the jet's entrainment.

Because of the different behaviour when compared to the experimental results, it is not meaningful to compute average values or evaluate the spreading of the jet in more detail. Nevertheless, the results show that INCA was successfully extended to be able to simulate supercritical jets, in particular Mayer's experiment. Three-dimensional simulations of the setup will be conducted in the future and results will be compared to experimental data as well as the results from other LES like project 1 and 3.

5. RGS with OpenFOAM (Project 3)

OpenFOAM (Open Field Operation and Manipulation [20]) is like SiTCom-B a finite volume code which solves a system of unsteady reacting Navier-Stokes equations on unstructured grids. In contrast to SiTCom-B, which solves density-based equations, OpenFOAM uses a pressure-based solution approach.

In low-Mach number flows, the linkage between pressure and density weakens, which makes the continuity an auxiliary condition more than a governing equation leading to a very stiff solver behaviour [21]. These problems can be handled by means of a proper preconditioning. A different approach to overcome this problem is a change in the system of governing equations. For incompressible flows a lot of solution algorithms have been developed which do not solve continuity directly, but a pressure equation developed from momentum and continuity instead. These so called pressure-based approaches have also been extended for compressible flows. The theory used in OpenFOAM is the compressible pressure-based PISO (Pressure Implicit with Splitting of Operators) algorithm which has been developed by Issa *et al.* [21, 22]. A second issue is a very strong time step restriction, which is driven by the speed of sound in conventional compressible flow solvers, leading to an enormous computational effort for low velocity flows. This limitation is weakened in OpenFOAM by a semi-implicit solution approach.

The numerical setup for the jet investigations has been chosen according to Schmitt *et al.* [23], where the chamber has been assumed to be rotationally symmetric. The geometry has been discretized using an o-grid with a total number of cells of about 1.7 million. The grid has been refined near the injector region. A detailed description of the grid can be found in figure 5. The grid on edges with arrow has been refined in this direction. The grid size near the injecter is between 0.1 mm and 0.15 mm.

Tab. 1 summarizes the initial conditions chosen for the investigations presented below. At the injector a time varying fully turbulent velocity profile extracted from a turbulent pipe flow is prescribed at the inlet. The top wall of the chamber is assumed to be adiabatic and the outer chamber walls temperature is set to 298 K. A wave transmissive boundary condition has been prescribed at the outlet. 2nd order centered differencing has been applied for spatial discretization and a first order implicit Euler scheme has been used for time integration.

Fig. 6 shows instantaneous Schlieren plots for case 3 and 4. As expected when regarding the coarser grid and the lower order spatial and time discretization, these results are more diffusive as the ones obtained with SiTCom-B. The general flow phenomena

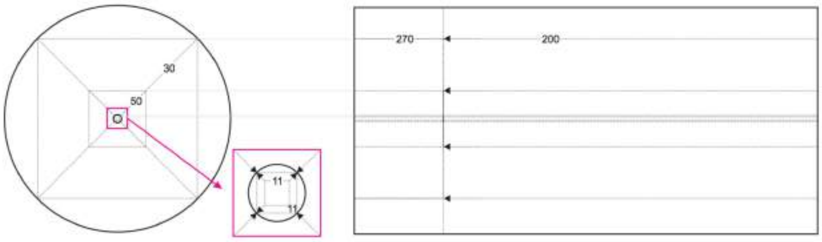

FIGURE 5. Grid for simulations of case 3 and 4 with OpenFOAM.

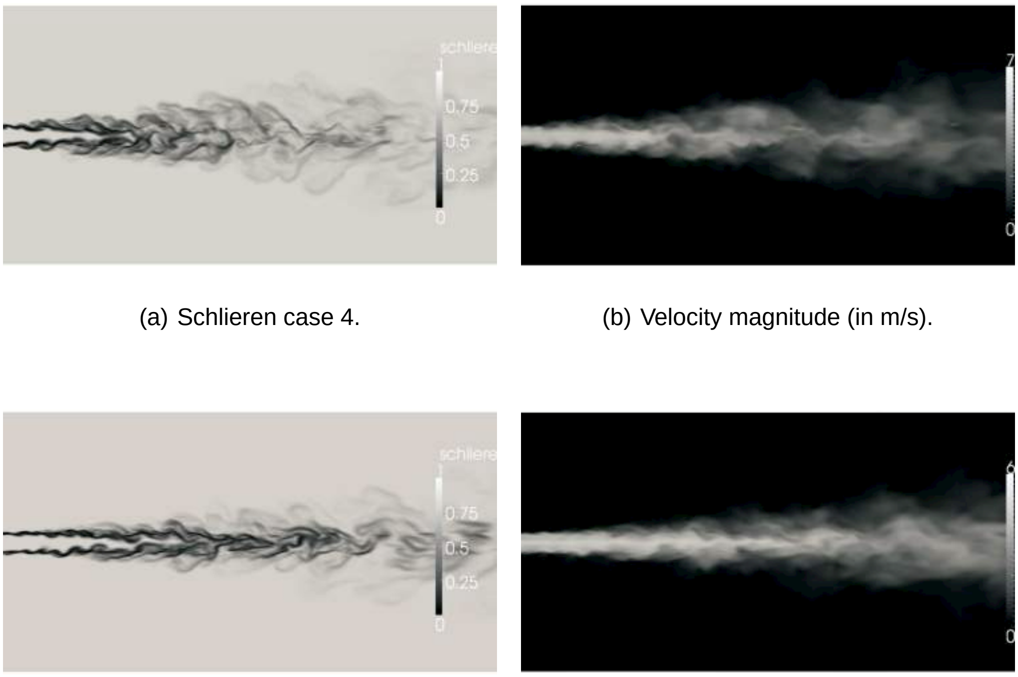

(a) Schlieren case 4.

(b) Velocity magnitude (in m/s).

(c) Schlieren case 3.

(d) Velocity magnitude (in m/s).

FIGURE 6. Simulation of case 3 and 4 with OpenFOAM.

however are captured very well using OpenFOAM. The same applies for the instantaneous plots of velocity magnitude.

6. Acoustic excitation of supercritical nitrogen jets (Project 4)

Combustion instabilities rise through the feedback of acoustic fluctuations to the heat release rate [24, 25] and may cause severe damages to the entire combustion system. Analysis and prediction of these instabilities in liquid rocket engines is still a crucial topic of research. A numerical tool, PIANO-SAT, has been developed at the *Lehrstuhl für Thermodynamik* of *Technische Universität München* for this purpose [26, 27]. As PIANO-SAT solves only the *Linearized Euler Equations*, the acoustic feedback, thus the fluctuating heat release rate, has to be modeled analytically. Crocco's n-τ-model, which correlates pressure and heat release fluctuations via a proportionality factor n and a time delay τ, is used for this purpose. A method has been developed to determine free parameters (e.g., n and τ) of analytical heat release models using CFD-simulations of single injectors instead of the whole injection plate with several hundreds of elements. Artificial excitation methods are used to impose a known acoustic field on the CFD-domains [28]. After previous tests with combustion of gaseous propellants [28], these methods have now been applied to a single nitrogen jet at supercritical temperatures and pressures. The aim was to test the excitation methods together with a real gas equation of state. Furthermore, some insights to the behavior of jets under acoustic excitation have been gained. Mayer's experiment is used as test case even if no data with acoustic excitation is available.

Simulations are carried out with *ANSYS CFX* using the URANS-equations with the k-ϵ-turbulence model and the PR EoS. The High Resolution Advection Scheme and a Second Order Backward Euler Transient Scheme have been used as well as the High Resolution Scheme for the turbulence. The High Resolution Scheme uses the second order schemes wherever and whenever possible and reverts to the first order schemes when it is required to maintain a bounded solution.

The computational domain consists of a 60 mm $\times$60 mm block with a length of 100 mm. A part of the cylindrical injector with a length of 10 mm is also included. The mesh has approximately 350,000 elements.

6.1. *Acoustic excitation method*

To force velocity perturbations in the domain, a harmonically fluctuating momentum source term, $\dot{s}_v$, is added to the transverse momentum balance equation as follows [28]:

$$\dot{s}_v = \bar{\rho}\hat{v}\omega\cos(\omega t)\,, \tag{6.1}$$

where the reference density, $\bar{\rho}$, is equal to the density at 300 K. This leads to a constant momentum source term in the whole domain, but to different velocity fluctuations in regions with different densities. Periodic conditions are applied for boundaries perpendicular to jet axis. As a consequence, velocity fluctuations in the domain do not yield any pressure fluctuations at the boundaries.

6.2. *Results*

Table 3 gives an overview of the different simulations realized with the injection conditions of case 4 (see Tab. 1). The indicated excitation amplitude corresponds to the value in the low density region. In the jet, the density being much higher, the velocity amplitude becomes much lower since a constant momentum source term is imposed in the whole domain.

Figure 7 shows six different excitation frequencies for the same excitation amplitude of 0.5 m/s (Cases 1-6, Tab. 3). Additionally, the steady solution is also shown for comparison. Iso-densities of 110 kg/m^3, the mean density between jet core and environment,

No.	f [Hz]	$\hat{v}$ [m/s]	Str	$\frac{\hat{v}}{u_{inj}}$
1	100	0.5	0.04	0.1
2	250	0.5	0.10	0.1
3	500	0.5	0.20	0.1
4	500	0.5	0.31	0.1
5	1,000	0.5	0.41	0.1
6	2,000	0.5	0.81	0.1
7	1,000	1.0	0.41	0.2
8	1,000	3.0	0.41	0.6
9	1,000	5.0	0.41	0.9

TABLE 3. Overview of the simulations; $Str = fd/u_{inj}$.

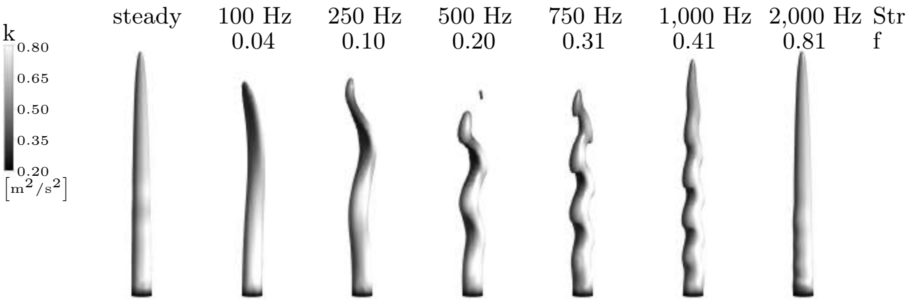

FIGURE 7. Comparison of different excitation frequencies.

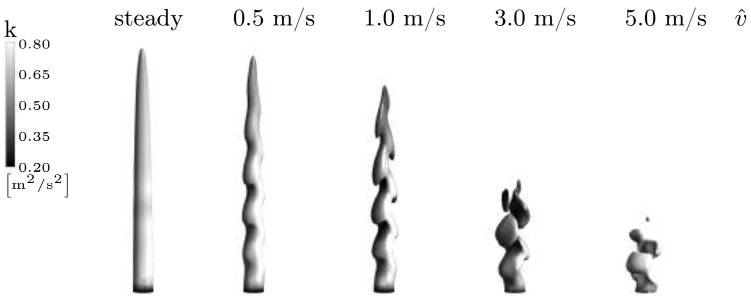

FIGURE 8. Comparison of different excitation amplitudes at 1,000 Hz.

are presented. They are gray scaled with the turbulence kinetic energy k. The most interaction between jet and acoustic is visible for a Strouhal-number of 0.2 – 0.3. The acoustic velocity fluctuations decrease the core length of the jet. Furthermore, they introduce alternating vortices at the injector exit. At lower frequencies, the convection time of disturbances is shorter than the oscillation period. Therefore, the jet just moves with the acoustic velocity fluctuations. Inversely, the acoustic oscillation period is too short compared to the convection time at higher frequencies. The strongest interaction of acoustics with jets at specific Strouhal-numbers has already been observed by other authors. It can be associated with a so called preferred mode of the jet [29, 30].

Figure 8 shows four different excitation amplitudes for the same excitation frequency of 1,000 Hz (Cases 5, 7-9, Tab. 3). Furthermore, the steady state solution is shown, too. The jet shortens considerably with an increasing acoustic excitation amplitude and it flattens perpendicular to the acoustic velocity fluctuations.

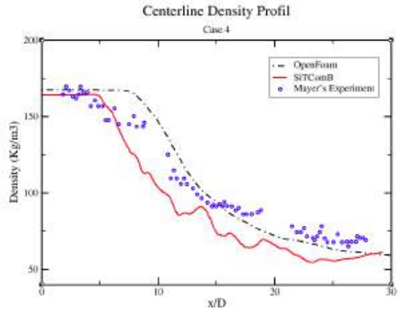

(a) Case 4.

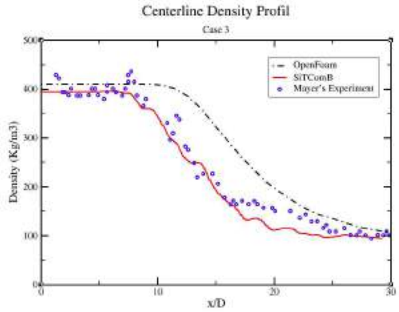

(b) Case 3.

FIGURE 9. Comparisons numerical results / experimental data for case 3 and 4.

A more detailed study of the interaction of acoustic velocity fluctuations with supercritical jets, including a quantitative analysis, will be performed in the future. The scaling of the interaction with excitation amplitude for constant Strouhal-numbers but different frequencies, diameters or injection velocities will be studied as well as the influence of acoustic pressure fluctuations on supercritical jets.

7. Conclusion

In Fig. 9 the mean axial density distribution from the LES is compared with experimental results from Mayer *et al.* [4]. The simulation of the near and supercritical injection show already good agreement with the experiment. For the near critical jet (case 3) the core length is predicted slightly too long. This indicates that the results calculated up to now are still too diffusive. Reasons for that can be found in the time integration scheme which has been only first order accurate in these investigations as well as in the rather coarse grid. In future investigations these topics will be improved.

A more detailed study of the interaction of acoustic velocity fluctuations with supercritical jets, including a quantitative analysis, should be performed in the future. It will be interesting to see the scaling of the interaction with excitation amplitude for constant Strouhal-numbers but different frequencies, diameters or injection velocities. Furthermore, the influence of acoustic pressure fluctuations on supercritical jets should also be studied.

Acknowledgments

Financial support has been provided by the German Research Foundation (Deutsche Forschungsgemeinschaft – DFG) in the framework of the Sonderforschungsbereich Transregio 40 and the IGSSE (International Graduate School of Science and Engineering) at Technische Universität München.

References

[1] CHEHROUDI, B., TALLEY, D. AND COY, E. (2002). Visual characteristics and initial growth rates of round cryogenic jets at subcritical and supercritical pressures. *Phys. Fluids*, **14**, 850.

[2] CHEHROUDI, B., COHN, R. AND TALLEY, D. (2002). Cryogenic shear layers: experiments and phenomenological modeling of the initial growth rate under subcritical and supercritical conditions. *Int. J. Heat Fluid Flow*, **23**(5), 554–563.

[3] MAYER W. AND TAMURA, H. (1996). Propellant injection in a liquid oxygen/gaseous hydrogen rocket engine. *J. Propul. Power*, **12**, 1137–1147.

[4] MAYER, W., TELAAR, J., BRANAM, R., SCHNEIDER, G. AND HUSSONG, J. (2003). Raman measurements of cryogenic injection at supercritical pressure. *Heat Mass Transfer*, **39**, 709–719.

[5] POLING, B. E., PRAUSNITZ, J. M. AND O'CONNELL, J. P. (2001). *The properties of gases and liquids.* 5th Ed., McGraw Hill.

[6] MENG, H. AND YANG, V. (2003). A unified treatment of general fluid thermodynamics and its application to a preconditioning scheme. *J. Comput. Phys.*, **189**, 277–304.

[7] BELLAN, J. (2000). Supercritical (and subcritical) fluid behavior and modeling: drops, streams, shear and mixing layers, jets and sprays. *Prog. Energ. Combust. Sci.*, **26**, 329–366.

[8] YANG, V. (2000). Modeling of supercritical vaporization, mixing, and combustion processes in liquid-fueled propulsion systems. *Proc. Combust. Inst.*, **28**, 925–942.

[9] CHUNG, T. H., AJLAN, M., LEE, L. L. AND STARLING, K. E. (1988). Generalized multiparameter corresponding state correlation for polyatomic, polar fluid transport properties. *Indust. Chem. Engin. Research*, **27**, 671–679.

[10] TAKAHASHI, S. (1974). Preparation of a generalized chart for the diffusion coefficient of gases at high pressures. *J. Chem. Engineering (Japan)*, **7**(6), 417–420.

[11] http://www.coria-cfd.fr/index.php/SiTCom-B

[12] RIBERT, G., TAIEB, D., PETIT, X., LARTIGUE, G. AND DOMINGO, P. (2011). Flow simulation under supercritical thermodynamics conditions. In: *Proc. 4th EUCASS*, St. Petersburg, Russia.

[13] PETIT, X., RIBERT, G. AND DOMINGO, P. (2012). Large Eddy Simulation of Supercritical Fluid Injection. In: *50th AIAA ASME Conf.*, *AIAA 2012–1268*, Nashville, TN, USA.

[14] HICKEL, S. AND LARSSON, J. (2008). An adaptive local deconvolution model for compressible turbulence. In: *Proc. CTR Summer Program 2008*, 85–96.

[15] http://www.inca-cfd.org/

[16] HICKEL, S. (2011). Implicit subgrid-scale modeling for Large Eddy Simulation of compressible flows and shock turbulence interaction. Submitted to *Phys. Fluids*.

[17] OKONG'O, N., HARSTAD, K. AND BELLAN, J. (2002). Direct Numerical Simulations of O_2/H_2 Temporal Mixing Layers Under Supercritical Conditions. *AIAA J.*, **40**(5), 914–926.

[18] NIEDERMEIER, C. A., HICKEL, S., ADAMS, N. A., JARCZYK, M. AND PFITZNER, M. (2011). Large Eddy Simulation of Oxygen/Hydrogen Mixing Layers under Supercritical Conditions. In: *Proc. 7th European Aerothermodynamics Symposium on Space Vehicles*, Brugge, Belgium.

[19] JARCZYK, M., PFITZNER, M., NIEDERMEIER, C. A., HICKEL, S. AND ADAMS, N. A. (2011). Large Eddy Simulation of Supercritical Mixing Layers. In: *Proc. 4th EUCASS*, St. Petersburg, Russia.

[20] WELLER, H., TABOR, G., JASAK, H. AND FUREBY, C. (1998). A tensorial approach to computational continuum mechanics using object-oriented techniques. *Computers in Physics*, **12(6)**, 620–631.

[21] ISSA, R. (1985). Solution of the implicitly discretised fluid flow equations by operator-splitting. *J. Comp. Phys.*, **62**, 40–65.

[22] ISSA, R., AHMADI-BEFRUI, B., BESHAY, K. AND GROSMAN, A. (1991). Solution of the implicitly discretised reacting flow equations by operator-splitting. *J. Comp. Phys.*, **93**, 388–410.

[23] SCHMITT, T., SELLE, L., RUIZ, A. AND CUENOT, B. (2010). Large-eddy simulation of supercritical-pressure round jets. *AIAA J.*, **48**(9), 2133–2144.

[24] HARRJE, D. T. AND REARDON, F. H. (Eds.) (1972). *Liquid Propellant Rocket Combustion Instability*. NASA SP-194.

[25] YANG, V. AND ANDERSON, W. E. (Eds.) (1995). *Liquid Rocket Engine Combustion Instability*. AIAA.

[26] MORGENWECK, D., FASSL, F., KAESS, R. AND SATTELMAYER, T. (2011). Influence of Scaling Rules on Loss of Acoustic Energy. *J. Spacecraft Rockets*, **48**(3), 498–506.

[27] PIERINGER, J. (2008). *Simulation selbsterregter Verbrennungsschwingungen in Raketenschubkammern im Zeitbereich*. PhD thesis, Lehrstuhl für Thermodynamik, Technische Universität München.

[28] SCHMID, M. AND SATTELMAYER, T. (2011). Influence of Pressure and Velocity Perturbations on the Heat Release Fluctuations for Coaxial GH2/GO2 Injection. In: *Proc. 4th EUCASS*, St. Petersburg, Russia.

[29] DAVIS, D. AND CHEHROUDI, B. (2004). The Effects of Pressure and Acoustic Field on a Cryogenic Coaxial Jet. In: *42nd AIAA ASME Conf.*, *AIAA 2004–1330*, Reno, NV, USA.

[30] GUTMARK, E. AND HO, C. (1983). Preferred modes and the spreading rates of jets. *Phys. Fluids*, **26**, 2932–2938.